Design of a Thermocapillary Flow Experiment in Reduced Gravity

Y. Kamotani* and S. Ostrach†
Case Western Reserve University, Cleveland, Ohio

Detailed considerations for the design of a low-gravity thermocapillary flow experiment are presented. The basic configuration is one in which a fluid contained in a circular dish is subjected to an imposed surface heat flux. Specific consideration is given to the imposed thermal signature, thermal boundary conditions, free-surface deformations, and *g*-jitter effects. Numerical analysis and ground-based and drop-tower tests are utilized to ensure that reasonable flows are obtained in which measurments can be made relatively easily. The configuration chosen is of further importance because it differs from others in which oscillations were observed.

Nomenclature

A = amplitude of container excitation
a = amplitude of free-surface deformation
D = container diameter
g = gravitational acceleration
g_0 = value of g on Earth's surface
H = liquid height
k = thermal conductivity
k_{mn} = wave number of surface deformation
Ma = Marangoni number
Pr = Prandtl number
R = container radius
r = radial coordinate defined in Fig. 2
T = temperature
To = cold wall temperature and also initial liquid temperature
T_H = heater temperature
Ts = temperature of free surface
t = time
U_s = velocity along free surface
α = absorptivity of liquid
ΔT = net temperature variation along free surface
ϵ = emissivity of heater
κ = thermal diffusivity of liquid
μ = viscosity
ν = kinematic viscosity
ρ = density of liquid
σ = surface tension
σ_0 = Stefan-Boltzmann constant
σ_T = $\partial\sigma/\partial T$
ψ = stream function
ω = frequency of oscillation
$\omega_{1,1}$ = natural frequency for sloshing mode

Introduction

THERMOCAPILLARY flow is driven by a thermally induced surface-tension variation along a liquid free surface. In the Earth-gravity environment, such flows are usually overshadowed by natural convection, but at reduced gravity conditions, their influence could be significant, as discussed by Ostrach.[1] For example, liquid free surfaces are inherent in the containerless processing of materials, so the effect of thermocapillary convection on the processing needs to be carefully assessed. A series of experiments on thermocapillary flows in space is being planned to determine their nature and extent. The present paper describes the work done to design the experiments.

The basic philosophy behind the experiments is as follows. Thermocapillary flow has already been demonstrated in space (e.g., Napolitano et al.[2]). The next step, then, is to obtain quantitative data by performing detailed experiments under controlled conditions and coupling the results with complementary numerical analysis. Also, observations have shown that thermocapillary flow becomes oscillatory under certain conditions (e.g., Preisser et al.[3]). Since the oscillation phenomenon has important implications for materials processing, it needs to be investigated in detail. The phenomenon has been demonstrated in space,[4] but there is a strong need for more quantitative study in order to gain a better understanding of it. In the past, we showed that the oscillation is associated with, among others, free-surface deformation (despite its smallness) and the corner regions (the regions near the hot and cold contact lines).[5] A quantitative study of both require sophisticated instruments, as well as more information on thermocapillary flow. Therefore, we proposed a series of three experiments in which we plan to investigate, step by step, thermocapillary flow and the associated oscillation phenomenon in detail.[6]

The present paper deals with the design of the first experiment, since the design of the second and third experiments depends heavily on what we learn in the first. In the first experiment, we will perform two tests: a one-hour test in which we will study the flow from its initial start-up to steady state and a half-hour test in which the heat input will be varied over a range to see if and when the flow becomes oscillatory.

In the first experiment, fluid (10-cs silicone oil) will be placed in a circular container and heated from above at the center to cause surface-tension variation in the radial direction (Fig. 1). The flow will be studied by observing tractor particles in the fluid through the sidewall, and the temperature field will be studied by several thermocouples placed in the fluid. The surface temperature distribution, which is important because it is directly related to the driving force of the flow, will be measured by a thermograph. In order to deal with more detailed design aspects, a numerical analysis of the flow has been made. In the analysis the effects of various boundary conditions on the flow, the effect of heater design and the amount of free-surface deformation are investigated. The analysis is discussed in the present paper. In conducting the experiment in space, it is essential that the liquid free surface is not much disturbed by g jitter aboard spacecraft. Thus, the deformation of the free surface due to g jitter has been analyzed, and it is also reported here.

Presented as Paper 86-0200 at the AIAA 24th Aerospace Sciences Meeting, Reno, NV, Jan. 6-9, 1986; received Jan. 27, 1986; revision received May 9, 1986.

*Associate Professor, Department of Mechanical and Aerospace Engineering. Member AIAA.

†Professor, Department of Mechanical and Aerospace Engineering. Fellow AIAA.

Experiment Design and Numerical Analysis

Basic Design

The basic experimental configuration is illustrated in Fig. 1. To obtain a nearly flat free surface, the test fluid is filled to the rim of the container. A heater in the middle imposes an axisymmetric heat flux along the free surface. The sidewall must be transparent for flow visualization.

Assuming that the free surface is flat and neglecting heat loss from the surface to the surrounding air, the important dimensionless parameters of the problem are: Marangoni number $Ma = \sigma_T \Delta T H/\mu\kappa$, Prandtl number $= Pr = \nu/\kappa$, and aspect ratio $= H/R$.

The above Ma is based on the temperature difference along the free-surface ΔT. Since the heat flux is specified at the free surface, it is more convenient to define Ma based on the heat flux, but the driving force of the flow is related to ΔT, not directly to heat flux, so the above Ma is used instead. It is noted that for given experimental conditions, Ma needs to be determined experimentally or by a numerical analysis.

The test fluid chosen is 10-cs silicone oil because it is transparent and safe and because its viscosity value is a reasonable compromise between a need for low viscosity to obtain a faster flow and a need for high viscosity to damp out small disturbances caused by g jitter. The aspect ratio has been chosen to be about unity so that the surface flow, as well as the corner flow, can be studied. It is desirable to select parametric ranges so that both nonoscillatory and oscillatory flow regimes are covered. However, the exact critical conditions for the transition are not known at present. Therefore, at least in the first experiment, we select values of Ma in the range of 10^4 to 10^5, the range in which the oscillations have been observed for the floating-zone configuration.[3] For this reason H and R are chosen to be 5 cm.

The main remaining design problems can be stated as follows:

1) Since the flow is to be observed through the sidewall, it would be convenient to make it an insulated wall so that it can be made from plastic and only the bottom wall is cooled. How is the flow affected by this?

2) As mentioned above, in the present configuration, Ma is not known a priori. If a cylindrical heater is placed inside the fluid at the center, we can impose ΔT along the surface and Ma is known. Is this better?

3) The temperature boundary-layer thickness along the free surface needs to be known accurately to find a proper way to measure the surface-temperature distribution.

4) Free-surface deformation is an important quantity in the oscillation mechanism. Is the amount of deformation large enough to be detected by flow visualization?

Numerical Analysis

To answer the above questions, we decided to perform a numerical analysis of the problem. The finite difference scheme used by Fu and Ostrach[7] to study thermocapillary flow in a simulated floating-zone configuration has been modified for the present configuration. A detailed description of the scheme is given in Fu and Ostrach.[7,8] A nonuniform grid system is employed, as illustrated in Fig. 2. Based on our past analysis of thermocapillary flow,[9] the length scale for the corner region, the region where the surface flow meets the sidewall and turns, is expected to be very small (of order Ma^{-1}) in the range of Ma studied herein ($= 10^4 - 10^5$). Numerically, it is extremely difficult to have such a small grid in the corner region, so some error in the numerical analysis is expected. Since the results from the present analysis are mainly used to help design the present experiment properly, $\pm 20\%$ accuracy is considered to be acceptable. In any case, it is very important to test some of the numerical results with ground-based experimental data. Based on such tests,[10] the grid system adopted in the present analysis in the range $Ma = 10^4 - 5 \times 10^4$ is a 40×40 mesh, with the smallest grid in the radial direction being 0.007 (relative to the radius) next to the sidewall and with the smallest grid in the axial direction being 0.01 next to the free surface. In the range $Ma = 6 \times 10^4 - 10^5$, a 50×50 mesh system is used, with the smallest grid in the radial direction being 0.006 and that in the axial direction being 0.008. Because the capillary number ($Ca = \mu U_s/\sigma$) is expected to be small in the proposed experiment ($Ca < 0.06$), it is reasonable to expect that the free-surface deformation due to fluid motion is relatively small so that the surface is assumed to be flat in the numerical analysis. After a flowfield is computed, the corresponding free-surface deformation is computed by domain perturbation.

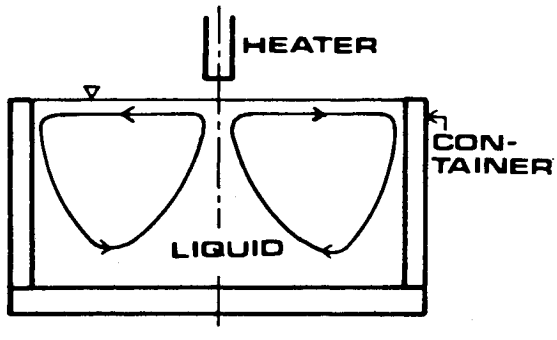

Fig. 1 Thermocapillary flow experiment.

Thermal Boundary Conditions

Three basic configurations, shown in Fig. 3, are studied numerically. In the first configuration, the side and bottom walls of the test cell are subjected to forced cooling and maintained at a fixed temperature. A radiant heater is placed above the liquid surface at the center. In the second configuration, the sidewall is not cooled to make flow visualization through the wall easier. The sidewall is considered to be either thermally insulated (if it is made of material such as plastic) or conductively connected to the bottom wall (if it is made of material such as sapphire). In the third configuration, a cylindrical heater is placed in the liquid in order to obtain a constant-temperature boundary condition at the heater side.

The liquid depth and radius are fixed at 5 cm. The test fluid is 10-cs silicone oil. All the physical properties of the fluid are considered to be invariant with temperature except the surface-tension variation with temperature. With a 10°C variation in temperature, the viscosity of silicone oil changes about 18%. Although the viscosity variation is not included in the present analysis because of the aforementioned accuracy needed in the analysis, its variation would have to be considered in a more accurate analysis.

For configurations I and II, the surface heat flux needs to be specified. In the present analysis, the heat flux is calculated based on the geometry, location, temperature, and emissivity ϵ of the heater and the absorptivity α of the liquid surface. Cylindrical heaters are considered to make the calculation of the shape factor between the heater and liquid surface easier. Three heaters of different lengths are considered, as shown in Fig. 4. The surface-heat flux becomes more diffuse with increasing heater length. The heater diameter is fixed at 1 cm, and it is placed at 5 mm above the surface. The computed heat-flux distributions corresponding to the three heater lengths are shown in Fig. 4. The value of α for silicone oil at room temperature is measured to be 0.92 in the spectral range 2-20 μm. The value of ϵ for the heater is taken to be 0.8.

In Fig. 5 the surface-temperature distributions at various Ma are presented for configuration I and heat flux I. Figure 5a shows the change of dimensionless surface-temperature profile with Ma. As Ma is increased and the convection along the surface becomes stronger, the profile becomes flatter and the temperature gradient at the sidewall increases. Dimensionally (see Fig. 5b), the overall temperature level increases with Ma. The fact that the temperature field becomes more uniform

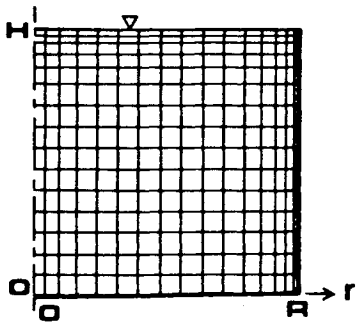

Fig. 2 Grid system for numerical analysis.

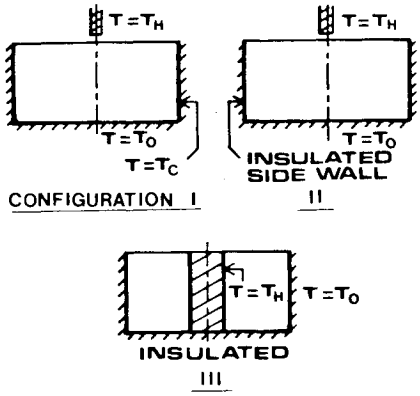

Fig. 3 Various configurations studied numerically.

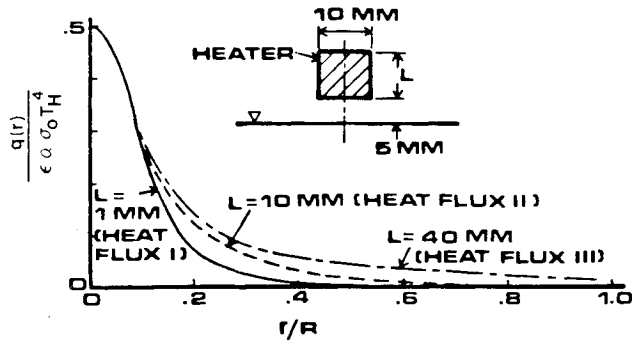

Fig. 4 Various surface heat-flux distributions studied numerically.

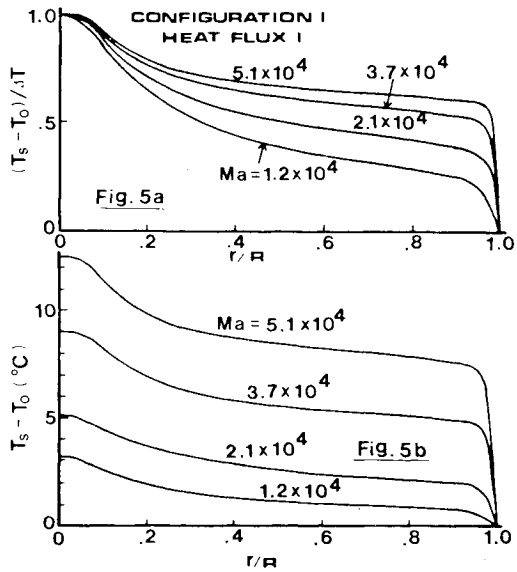

Fig. 5 Effect of *Ma* on surface-temperature distribution.

with greater convection makes it increasingly difficult to increase the value of *Ma*. For example, to change *Ma* from 1.2×10^4 to 4.9×10^4 (fourfold difference) requires an increase of more than 25 times in the heat flux from the heater.

The surface-velocity distributions corresponding to the above temperature distributions are shown in Fig. 6. Figure 6a shows that the nondimensionalized velocity decreases with increasing *Ma* due to the aforementioned flattening of the surface-temperature profile. As a result, the dimensional velocity (Fig. 6b) does not increase rapidly with *Ma*. The average velocity is of order 10-20 cm/min, which is in a proper range for flow visualization.

Temperature and velocity distributions near the free surface are shown in Fig. 7. Because of the existence of a thermal boundary layer along the surface, the temperature decreases sharply with depth in the layer. The boundary layer is thinnest at the center and the temperature gradient there is of order 6°C/mm at $Ma=5\times10^4$. The average thickness of the thermal boundary layer is of order 1 mm. Those factors need to be considered in choosing a method to measure the surface temperature. The surface-layer thickness for the velocity is larger than the temperature boundary-layer thickness and it is of order 5-10 mm.

Figure 8 shows the amounts of free-surface deformation due to thermocapillary flow for various values of *Ma*. The surface is assumed to be anchored at the edge, so the maximum deformation is at the center. The deformation increases sharply with *Ma*, but the magnitude of deformation is relatively small within the range of *Ma* studied (0.5 mm, or 1% of the fluid depth, at $Ma=8.8\times10^4$), which means an elaborate optical system is needed to study the deformation.

The effects of various surface heat-flux profiles (heat fluxes I, II, and III in Fig. 4) on the surface-temperature and velocity distributions are shown in Fig. 9. As seen in Fig. 9a, with *Ma* kept nearly constant, a concentrated heat flux (I) causes a relatively large temperature variation along the surface. Consequently, the maximum surface velocity is obtained near the center for heat flux I. In contrast, for heat flux III, the temperature profile is relatively flat over most of the surface but has a large temperature variation near the wall and, as a result, the maximum velocity occurs near the wall. Experimentally, it is not desirable to have such a concentrated driving force because of the difficulty in investigating the relationship between the surface-temperature and velocity distribution

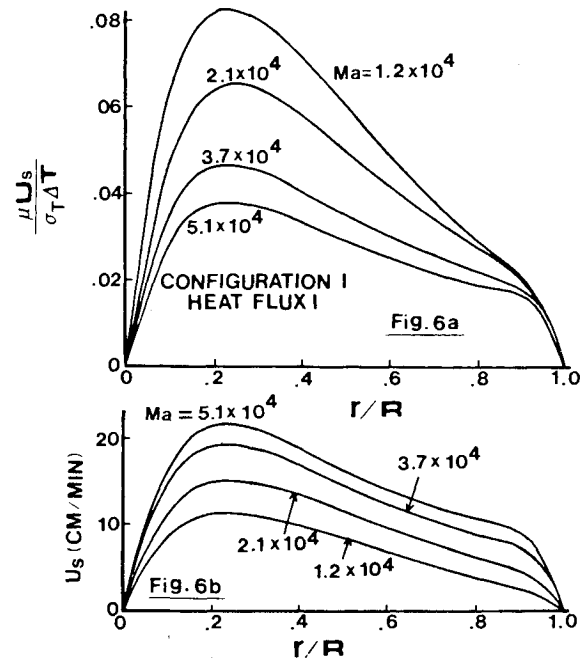

Fig. 6 Effect of *Ma* on surface-velocity distribution.

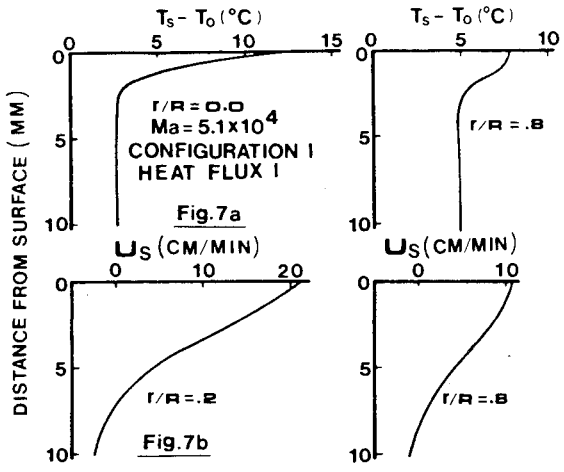

Fig. 7 Temperature and velocity distributions in liquid.

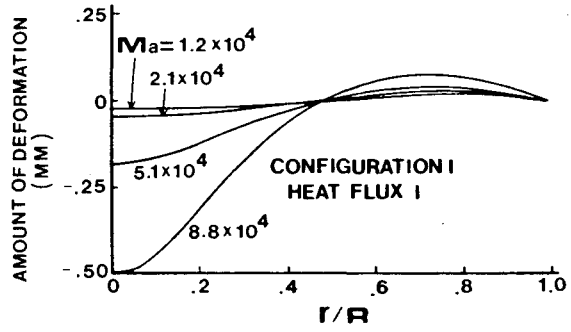

Fig. 8 Free surface deformation.

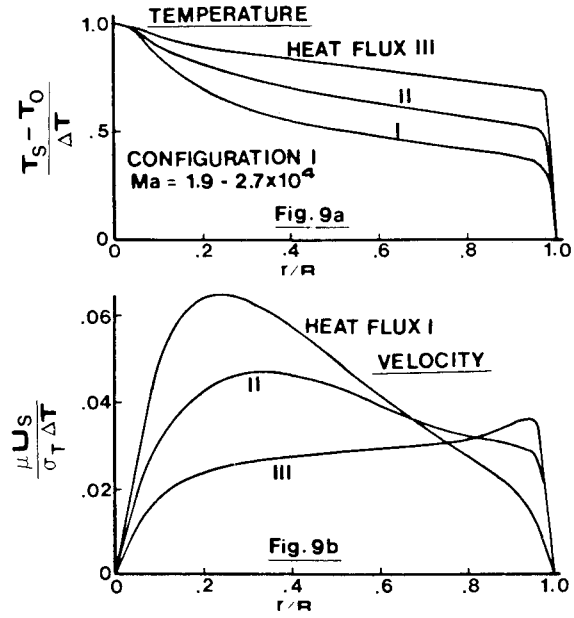

Fig. 9 Effect of heat-flux distribution on surface-temperature and velocity distributions.

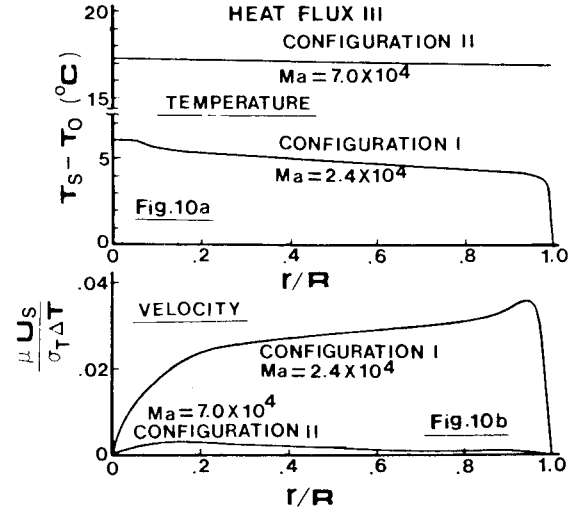

Fig. 10 Effect of insulated sidewall on surface-temperature and velocity distributions.

and, moreover, the region close to the wall is strongly influenced by the complex behavior of the contact line. For those reasons, in the proposed first experiment, a relatively concentrated heat flux such as heat flux I will be considered.

As for the effects of experimental configuration on the flow, configuration II with an insulated sidewall (see Fig. 3) is compared with configuration I in Fig. 10. With the sidewall insulated, the surface temperature is made nearly flat by convection (Fig. 10a) and, as a result, the surface velocity becomes very small (Fig, 10b). Obviously, configuration II with an insulated sidewall is not appropriate for the proposed experiment.

Configuration II with a conducting sidewall is a different matter. Two sidewall materials, glass and sapphire, are considered. The thermal conductivities of sapphire and glass relative to that of the test fluid are 285 and 7.7, respectively. As Fig. 11 shows, a glass wall acts almost like an insulating wall. With a sapphire sidewall, the velocity and temperature distributions are close to those for the cooled sidewall. Thus, configuration II with a sapphire sidewall is considered acceptable for the proposed experiment.

Configuration II with a conducting sidewall is a different matter. Two sidewall materials, glass and sapphire, are considered. The thermal conductivities of sapphire and glass relative to that of the test fluid are 285 and 7.7, respectively. As Fig. 11 shows, a glass wall acts almost like an insulating wall. With a sapphire sidewall, the velocity and temperature distributions are close to those for the cooled sidewall. Thus, configuration II with a sapphire sidewall is considered acceptable for the proposed experiment.

Typical velocity and temperature distributions for configuration III are presented in Fig. 12. The heater radius is 10% of the container radius. The surface temperature drops sharply near the heater and less sharply near the sidewall. Consequently, the maximum velocity is obtained near the heater. As mentioned above, such a strong concentration of driving force in small regions is not very desirable experimentally because of the difficulty in determining the temperature distributions in such small regions.

Transient Effects

In order to determine how long it takes for the flow to become steady, a transient flow analysis has been conducted starting from a quiescent, uniform temperature state. Typical transient flow behaviors are shown in Fig. 13. The heater temperature is assumed to take 2½ min to become steady. Temperature variations at four locations following the flow development are shown in Fig. 13a. The region in which it takes longest to become steady is the region near the center and outside the surface thermal boundary layer (location D in Fig. 13a). It takes about one hour after the heater is turned on for the temperature field to become steady. The velocity field becomes steady sooner than the temperature field, not only because *Pr* is large but because the surface-temperature distribution near the center (related to the main driving force) is established quickly. As Fig. 13b shows, the overall velocity

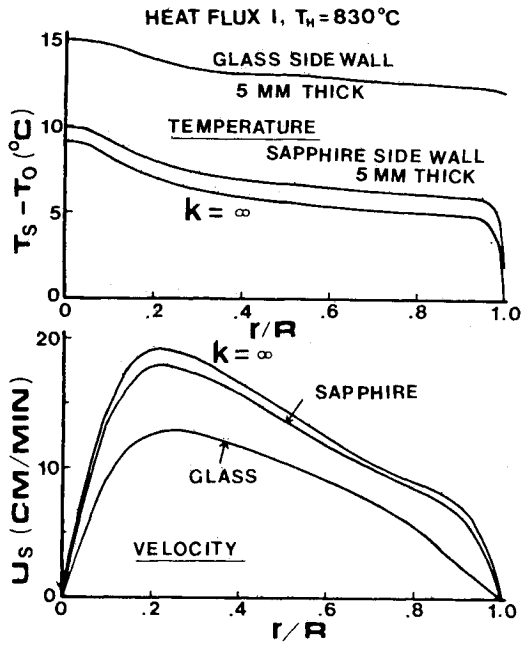

Fig. 11 Effect of sidewall conduction on surface velocity and temperature distributions.

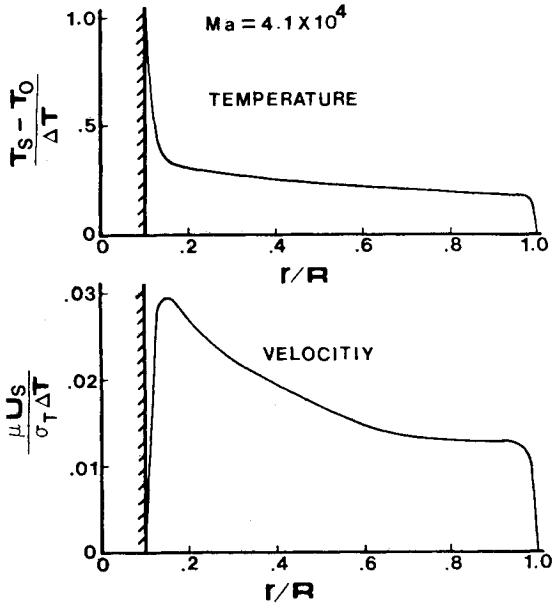

Fig. 12 Surface-velocity and temperature distributions for configuration III.

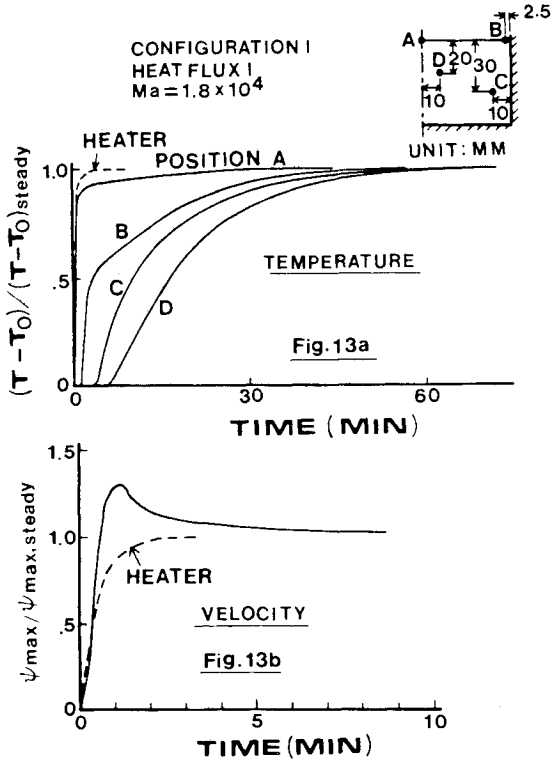

Fig. 13 Transient temperature and velocity variations.

field, represented by the value of maximum stream function ψ_{max}, is considered to become steady about 10 min after the heating is started. Because a relatively large temperature gradient exists near the center for some time after the heating, ψ_{max} overshoots its steady value and then gradually decreases as the surface flow reduces the temperature gradient near the center.

In summary, configuration I is preferred over configuration III, configuration II is acceptable if the sidewall is made of sapphire, the surface thermal boundary-layer thickness is of order 1 mm, the amount of free-surface deformation is less than 0.5 mm, and it takes about an hour for the temperature field to become steady.

Effect of *g* Jitter on Free Surface

To investigate the effect of *g* jitter on the liquid free surface under reduced gravity, an analysis of the data obtained in relevant past work and drop-tower tests has been conducted. In the present work, *g* jitter is simulated by sinusoidal vibration of a liquid-filled cylindrical container. The direction of the vibration is either in the direction normal to the free surface or in the direction parallel to the free surface.

The drop-tower tests were conducted in the 85-ft drop-tower facility at NASA Lewis Research Center.[10] Since the duration of reduced gravity in the drop tower was only about 2 s and the impact at the bottom was large ($-25\ g_0$), no elaborate tests were possible, so we had to rely mainly on the analysis of available data on free-surface instability.

The subject of liquid free-surface motion under normal or parallel excitation was extensively studied during the early 1960s in connection with liquid sloshing in liquid-fuel rockets. The work up to 1963 was reviewed by Abramson.[11] Not much has been done since then on parallel excitation, but recently Gollub and Meyer[12] and Ciliberto and Gollub[13] studied the problem of normal excitation in convection with symmetry-breaking instabilities leading to chaos.

As for the excitation normal to the free surface, it is known to be a stability problem, that is, the free surface deforms only under certain conditions. The amplitude of *g* jitter is very small (less than $10^{-3}\ g_0$) so that it can be shown that the free surface becomes unstable only near the natural frequencies.[10] As discussed by Abramson,[11] the most unstable mode experimentally is the one-half-subharmonic mode in which the surface oscillation frequency is half the excitation frequency, which means that for the present experimental conditions, the lowest excitation frequency for surface instability is expected to be about 0.8 Hz.

Theoretically, an infinitesimal *g* level is sufficient to make the surface unstable at the natural frequencies, but in practice the effect of viscosity can damp out small disturbances so that a finite *g* level is required to make the surface unstable near the natural frequencies. This minimum *g* level is our main interest in this study. Although there are some experimental data available for the minimum *g* level,[12,14] they need to be correlated in order to extrapolate them to the proposed experimental conditions. Since such analysis has not been done in the past, it is developed herein.

Based on an analogy to a mechanical spring-mass-viscous damper system subjected to forced oscillations (force $= P_0 \sin \omega t$), it can be said that at a natural frequency the surface becomes unstable if the ratio of the surface oscillation amplitude to the static amplitude (corresponding to P_0) becomes larger than a certain critical value that depends on viscous damping. If the excitation force is given as $A\omega^2 \sin \omega t$, the above ratio can be shown to scale with the Bond number based on $A\omega^2$, namely, $\rho A\omega^2/\sigma k_{mn}^2$, where k_{mn} is the wave number of surface deformation or, if the effect of gravity on the restoring force is included, $\rho A\omega^2/(\rho g + \sigma k_{mn}^2)$. Thus, in order to have an unstable system

$$\rho A\omega^2/(\rho g + \sigma k_{mn}^2) > \text{Viscous damping}$$

According to Case and Parkinson,[15] the effect of viscous damping in the bulk fluid is a function of the dimensionless parameter $\mu\nu k_{mn}^3/(\rho g + \sigma k_{mn}^2)$. Therefore, the minimum g level for the surface instability near a natural frequency can be expressed as

$$\frac{\rho(A\omega^2)_{\min}}{\rho g + \sigma k_{mn}^2} = f_n\left(\frac{\mu\nu k_{mn}^3}{\rho g + \sigma k_{mn}^2}\right) \tag{1}$$

Available experimental data on the minimum g levels are correlated according to Eq. (1) in Fig. 14. Although the data were taken in 1 g, the tests covered both gravity-dominant situations ($\rho g/\sigma k_{mn}^2 > 1$) and surface-tension dominant situations ($\rho g/\sigma k_{mn}^2 < 1$). As seen in Fig. 14, the data can be correlated reasonably well by Eq. (1). According to the best-fitting curve,

$$\frac{\rho(A\omega^2)_{\min}}{\rho g + \sigma k_{mn}^2} = 0.33\left(\frac{\mu\nu k_{mn}^3}{\rho g + \sigma k_{mn}^2}\right)^{.11} \tag{2}$$

Based on Eq. (2), the minimum g level for the proposed experimental condition is calculated and shown in Fig. 15. The result is applicable only at the natural frequencies, but it is shown as a continuous line for simplicity. As Fig. 15 shows, if the g level is maintained at $10^{-4}\ g_0$ or less during the proposed experiment, the surface is considered to be quite stable against g jitter in the direction normal to the free surface.

In the case of excitation parallel to the free surface, the surface deforms whenever it is subjected to g jitter, and the dominant mode is a simple sloshing mode. The natural frequency corresponding to that mode is calculated to be about 0.4 Hz for the proposed experimental conditions in reduced gravity. At the natural frequency, the kinetic energy of liquid motion is balanced by the surface energy to maintain a steady oscillation in reduced gravity. If, then, the system is excited at the natural frequency, it breaks the balance, and the free-surface deformation increases without bound. However, the effect of viscosity does not allow the amplitude to become infinite. The amplitude of oscillation at the natural frequency for a given excitation force and test conditions does not seem to have been analyzed in the past, so a relatively simple analysis is given herein.

As mentioned above, during oscillation at the natural frequency, the kinetic energy is balanced by the surface energy, so the external force, if applied, must be balanced by the viscous forces. Physically, the excitation induces a pressure field in the container in such a way as to cause a sloshing motion of liquid, and this total pressure force needs to be balanced by the total viscous forces at the natural frequency. When the oscillation Reynolds number $\omega D^2/\nu$ is large, as in the proposed experiment, there is a viscous boundary layer along the sidewall of thickness $\sqrt{\nu/\omega}$. With the container aspect ratio (radius/depth) equal to unity, the liquid motion does not reach the bottom wall. Therefore, if the free-surface amplitude is given as $a\omega \sin \omega t$, the viscous stress at the wall can be estimated as $\mu a\omega/\sqrt{\nu/\omega}$. The pressure induced by the excitation $A\omega^2 \sin \omega t$ scales with $\rho A\omega^2 D$. By balancing the above two forces, we have

$$\mu a\omega/\sqrt{\nu/\omega} \sim \rho A\omega^2 D$$

or

$$a^2/D^2 \sim A^2\omega/\nu \quad \text{at } \omega = \omega_{1,1}$$

where $\omega_{1,1}$ is the natural frequency for the sloshing mode. The proportionality constant of the above equation was determined in the drop-tower tests, and we obtained

$$a/D = 0.16(A^2\omega/\nu)^{1/2} \tag{3}$$

According to Eq. (3), for $\omega = 0.4$ Hz, $A\omega^2 = 10^{-4}\ g_0$, $D = 10$ cm, and 10-cs silicone oil, the amplitude of the free-surface oscillation is calculated to be 1.2 mm. The amount is considered to be slightly excessive, but it is noted that the above estimate is based on the assumption that g jitter of magnitude $10^{-4}\ g_0$ occurs only near $\omega = 0.4$ Hz. In reality, the spectral distribution of g jitter is considered to be much more diffuse, and the free-surface deformation associated with $\omega = 0.4$ Hz is much less than the above estimate.

In summary, the effect of g jitter is considered to be negligible if g-jitter level is $10^{-4}\ g_0$ or less.

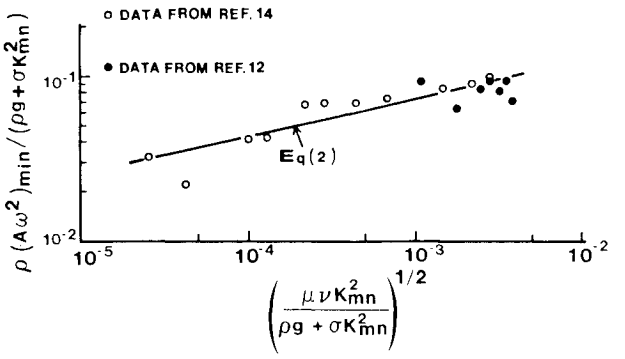

Fig. 14 Minimum g level vs viscous damping.

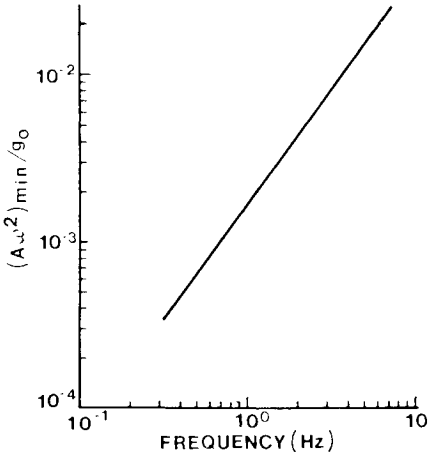

Fig. 15 Minimum g level for surface instability.

Concluding Remarks

The space flight experiment described herein in which a fluid in a circular dish is subjected to an imposed surface heat flux is particularly well suited to study thermocapillary flows and their oscillations because we have considerable ground-based experience with such an apparatus, the nature of the flows makes measurements easier, and the configuration is different from any others in which oscillations were observed.

Acknowledgments

This work was performed through the sponsorship of NASA Lewis Research Center and monitored by T. Jacobson.

References

[1]Ostrach, S., "Low-Gravity Fluid Flows," *Annual Review of Fluid Mechanics*, Vol. 14, 1982, pp. 313-345.

[2]Napolitano, L. G., Monti, R., and Russo, G., "Some Results of the Marangoni Free Convection Experiment," *Proceedings of the 5th European Symposium on Material Sciences under Microgravity*, ESA Report SP-222, Schloss Elmau, Germany, Nov. 1984, pp. 15-22.

[3]Preisser, F., Schwabe, D., and Scharmann, A., "Steady and Oscillatory Thermocapillary Convection in Liquid Columns with Free Cylindrical Surface," *Journal of Fluid Mechanics*, Vol. 126, Jan. 1983, pp. 545-567.

[4]Schwabe, D. and Scharmann, A., "Measurements of the Critical Marangoni Number of the Laminar-Oscillatory Transition of Thermocapillary Convection in Floating Zones," *Proceedings of the 5th European Symposium on Material Sciences under Microgravity*, ESA Report SP-222, Schloss Elmau, Germany, Nov. 1984, pp. 281-289.

[5]Ostrach, S., Kamotani, Y., and Lai, C-L., "Oscillatory Thermocapillary Flow," *Physico Chemical Hydrodynamics*, Pergamon Press, Vol. 6, No. 5/6, 1985, pp. 585-599.

[6]Ostrach, S. and Kamotani, Y., "Science Requirements Document for Surface Tension Driven Convection Experiment in Reduced Gravity," Report to NASA, Case Western Reserve University, Cleveland, OH, May 1985.

[7]Fu, B-I. and Ostrach, S., "Numerical Solutions of Thermocapillary Flows in Floating Zones," *Transport Phenomena in Materials Processing*, ASME HTD-Vol. 29, 1983, pp. 1-9.

[8]Fu, B-I. and Ostrach, S., "Numerical Solutions of Floating Zone Crystal Growth," Rept. FTAS/TR-82-169, Case Western Reserve University, Cleveland, OH, Jan. 1983.

[9]Lai, C-L., Ostrach, S., and Kamotani, Y., "Studies of Thermocapillary Oscillation Phenomena," Rept. FTAS/TR-84-177, Case Western Reserve University, Cleveland, OH, Aug. 1984.

[10]Ostrach, S. and Kamotani, Y., "Additional Study for Science Requirements Document for Surface Tension Driven Convection Experiment in Reduced Gravity," Report to NASA, Case Western Reserve University, Cleveland, OH, April 1985.

[11]Abramson, H. N., "Dynamic Behavior of Liquid in Moving Container," *Applied Mechanics Review*, Vol. 16, July 1963, pp. 501-506.

[12]Gollub, J. P. and Meyer, C. W., "Symmetry-Breaking Instabilities on a Fluid Surface," *Physica*, Vol. 6D, 1983, pp. 337-346.

[13]Ciliberto, S. and Gollub, P., "Pattern Competition Leads to Chaos," *Physical Review Letters*, Vol. 52, March 1984, pp. 922-925.

[14]Dodge, F. T., Kana, D. D., and Abramson, H. N., "Liquid Surface Oscillations in Longitudinally Excited Rigid Cylindrical Containers," *AIAA Journal*, Vol. 3, April 1965, pp. 685-695.

[15]Case, K. M. and Parkinson, W. C., "Damping of Surface Waves in an Incompressible Liquid," *Journal of Fluid Mechanics*, Vol. 2, March 1957, pp. 172-184.